Science of the Total Environment 414 (2012) 564–575

Contents lists available at SciVerse ScienceDirect

Science of the Total Environment

journal homepage: www.elsevier.com/locate/scitotenv

Black soiling of an architectural limestone during two-year term exposure to urban air in the city of Granada (S Spain)

Maja Urosevic [a,*], Africa Yebra-Rodríguez [b], Eduardo Sebastián-Pardo [a], Carolina Cardell [a]

[a] Dept. Mineralogy and Petrology, Faculty of Science, University of Granada, Campus Fuentenueva s/n, 18071 Granada, Spain
[b] Dept. Geology-Associated Unit IACT (CSIC-UGR), Faculty of Experimental Science, University of Jaén, Campus Las Lagunillas s/n, 23071 Jaén, Spain

ARTICLE INFO

Article history:
Received 3 June 2011
Received in revised form 16 October 2011
Accepted 10 November 2011
Available online 5 December 2011

Keywords:
Building limestone
Black soiling
Air pollution
Atmospheric particles
Spectrophotometry
Architectural heritage

ABSTRACT

A two-year term aging test was carried out on a building limestone under different urban conditions in the city of Granada (Southern Spain) to assess its Cultural Heritage sustainability. For this purpose stone tablets were placed vertically at four sites with contrasting local pollution micro-environments and exposure conditions (rain-sheltered and unsheltered). The back (rain-sheltered) and the front (rain-unsheltered) faces of the stone tablets were studied for each site. The soiling process (surface blackening) was monitored through lightness (ΔL^*) and chroma changes (ΔC^*). Additionally atmospheric particles deposited on the stone surfaces and on PM10 filters during the exposure time were studied through a multianalytical approach including scanning electron microscopy (SEM-EDX), transmission electron microscopy (TEM) and micro-Raman spectroscopy. The identified atmospheric particles (responsible for stone soiling) were mainly soot and soil dust particles; also fly ash and aged salt particles were found. The soiling process was related to surface texture, exposure conditions and proximity to dense traffic streets. On the front faces of all stones, black soiling and surface roughness promoted by differential erosion between micritic and sparitic calcite were noticed. Moreover, it was found that surface roughness enhanced a feedback process that triggers further black soiling. The calculated effective area coverage (EAC) by light absorbing dust ranged from 10.2 to 20.4%, exceeding by far the established value of 2% EAC (limit perceptible to the human eye). Soiling coefficients (SC) were estimated based on square-root and bounded exponential fittings. Estimated black carbon (BC) concentration resulted in relatively similar SC for all studied sites and thus predicts the soiling process better than using particulate matter (PM10) concentration.

1. Introduction

Stone decay in polluted urban atmosphere is an outstanding problem with paramount cultural and economic consequences that have attracted the attention of extensive research during decades (see Doehne and Price, 2010 for a comprehensive review). In fact, the effect of air pollution on stone decay is still a major problem even though acidic pollutant levels have considerably decreased since the early 1990s (Doehne and Price, 2010). The danger to Cultural Heritage from air pollution comes from several main sources such as increasing corrosion induced by gases from the atmosphere (Charola and Ware, 2002; Cardell-Fernández et al., 2002; Sabbioni, 2003), soiling of light-colored stone surfaces due to black particles, i.e. black soiling (e.g. Grossi et al., 2003; Hamilton and Crabbe, 2009), and crystallization of soluble and insoluble salts inside the porous network that eventually leads to stone disaggregation and surface recession (Scherer, 1999; Doehne, 2002 and references therein). Moreover, surface recession can be also enhanced by the occurrence of sulfates and nitrates as a consequence of the rain effect (Sabbioni and Zappia, 1992; Bonazza et al., 2009; Siegesmund and Snetlage, 2011). The development of black crusts is a well-known process associated with surface deposition of complex mixtures of atmospheric particles and gases derived from the combustion of fossil fuels together with varieties of environmental dust, salts including marine aerosols, and microbial fauna (Watt et al., 2009 and references therein). The blackness of these gypsum crust layers is commonly explained by absorption of carbonaceous particles such as soot (e.g. Sabbioni and Zappia, 1992). Additionally, it has been argued that carbon soot and metal-rich particles (e.g. V, Fe, Ni, Cu, Mn and Cr-rich particles derived from anthropogenic sources) catalyze the oxidation of SO_2 (Camuffo et al., 1984; Rodríguez-Navarro and Sebastián-Pardo, 1996; Maravelaki-Kalaitzaki and Biscontin, 1999; Böke et al., 1999, 2002; Maravelaki-Kalaitzaki, 2005), although the additional catalytic effect of bacteria is not discarded. Further assessment of the link between anthropogenic activities and black soiling has been provided by quantitative data of organic and elemental carbon (OC and EC) in damage layers on historic buildings worldwide (Sabbioni and Zappia, 1992; Sabbioni et al., 2003; Bonazza et al., 2005, 2007; Ghedini et al., 2006).

* Corresponding author. Tel.: +34 958 246614; fax: +34 958 243368.
E-mail address: maja@ugr.es (M. Urosevic).

0048-9697/$ – see front matter © 2011 Elsevier B.V. All rights reserved.
doi:10.1016/j.scitotenv.2011.11.028

One approach followed to address the above issues combines detailed observations of already weathered construction materials from polluted cities with *ad hoc* experiments under controlled laboratory conditions (e.g. Rodríguez-Navarro and Sebastián, 1996; Simão et al., 2006). Experimental data are later extrapolated to 'real' urban conditions. The diversity of tested stone materials under different environmental conditions has provided considerable understanding of their main weathering mechanisms. However to ensure measurable results in relatively short times, these experiments are usually conducted under extreme environmental conditions which are usually far from those prevailing in urban conditions. Therefore a direct extrapolation to natural conditions is not straightforward and leads to several uncertainties in the estimation of decay rates, which are an important issue in the sustainability of Cultural Heritage. Furthermore many factors both intrinsic (stone-related properties) and extrinsic (environmental-related variables such as exposure and micro climatic conditions, pollution, etc.) are still challenging to be reproduced experimentally.

For these reasons, an important amount of research has been focused on field tests in order to address long-term sustainability of architectural materials (e.g. Delalieux et al., 2002; Viles et al., 2002; Sabbioni, 2003; Viles and Gorbushina, 2003; Grossi et al., 2003, 2007). Pioneering long-term field aging tests designed to study the soiling effect of atmospheric aerosols on building stones were conducted by Beloin and Haynie (1975) using changes in reflectance to asses the stone weathering process. Similar studies were carried out by Creighton et al. (1990), Hamilton and Mansfield (1992) and Pio et al. (1998), which discussed several fitting equations of experimental data relating decreased reflectance to exposure time. Further systematic research has been carried out to develop robust fitting parameters of larger dataset with the aim to improve dose–response functions (Brimblecombe and Grossi, 2004; Kucera, 2005) which are appropriate for long-term predictions of soiling. Although to be essential to design conservation policies of vulnerable Cultural Heritage legacy (Grossi and Brimblecombe, 2004; Brimblecombe and Grossi, 2004, 2005, 2007, 2009), these kinds of studies are still limited to few places around Europe (Grossi and Brimblecombe, 2007).

This study is aimed to investigate the black soiling of a carbonate stone (i.e. a porous limestone used to replace similar historic carbonate stones in monuments in Andalusia, South Spain) under Granada urban conditions during a two-year term exposure test (period of 2008 and 2009). The city of Granada is considered a relatively non-polluted city in terms of NO_x, CO, SO_2 and O_3 (average values are below the EU normative) but significantly exceeds the EU normative limit values for particulate matter concentration (PM10) even if the effect of frequent mineral dust-rich Saharian intrusion is discounted (Lyamani and Bravo Aranda, 2009, 2010; Kontozova-Deutsch et al., 2011). Therefore most of the architectural heritage of Granada, built with carbonate stones, is rather prone to weathering and darkening under its urban conditions. Assessment of soiling was qualitatively and quantitatively estimated by chromatic changes at the porous limestone surfaces through spectrophotometric measurements. Additionally, atmospheric particles deposited on the stone surfaces and filters were analyzed by scanning electron microscopy (SEM), transmission electron microscopy (TEM) and micro-Raman spectroscopy (MR). Based on observed lightness changes (ΔL^*) the effective area covered by dark particles (EAC) was estimated. Moreover, soiling coefficients were determined by assuming several empirical models.

2. Materials and methods

2.1. Materials

A porous limestone (carbonate stone) from the *Escúzar* quarry situated ~20 km to the SW of the city of Granada, Southern Spain (Urosevic et al., 2011) was selected for this study. The main constituents (>80–90 vol.%) of this limestone are fossil fragments (allochemical component). Fragments of bioclasts include molluscs, echinoderms, briozoan, red algae and foraminifera. The allochemical grain size ranges from 1 mm to 4 mm (Urosevic et al., 2011) thus the geological term biogenic calcirudite is preferred in most of the cases. Following Folk's scheme *Escúzar* limestone is classified as 'sparry biogenic calcarenite/calcirudite' or simply 'biosparite/biorudite' (Folk, 1981). This stone is texturally very heterogeneous, highly porous ($29.30 \pm 7.6\%$ on average) and scarcely cemented (sparry and micritic calcitic cement). These features, together with the high calcite proportion in its matrix, make this stone very prone to weathering under polluted environments by dissolution processes induced by acid rain and gypsum crust formation. Moreover the lower grain size of the micritic calcite in the matrix and therefore its high specific surface area enhances calcite dissolution in the matrix compared the less reactive sparitic domains. This process commonly leads to desegregation and differential surface erosion, typical of bioclastic limestones (such as the *Escúzar* porous limestone).

This porous limestone is commonly used in modern architecture in Andalusia as well as in monuments replacing the historic *La Escribana* bioclastic calcarenite widely used in ancient buildings of the city of Granada such as the Cathedral, the Charles V Palace and the San Jerónimo Monastery (Rodríguez-Navarro, 1994; Rodríguez-Navarro and Sebastián, 1996; Cardell, 1998; Cardell et al., 2008; Rodríguez-Navarro et al., 2008).

2.2. Environment and sample location

Granada is a non-industrialized, medium-sized city in Southern Spain with a population of around 300,000 (double for the entire urban area). It is about 50 km from the Mediterranean Sea and around 200 km from the African continent. Granada is located in an intraorogenic basin surrounded by mountains with the highest elevations (up to 3500 m) located to the southeast. Due to its topography in combination with the prevailing low wind speeds, heavy traffic and intensive construction works (e.g. Metropolitan works during the test period of 2008 and 2009), pollutants and soot particles often accumulate in the air of Granada. Indeed, around 9% of black carbon (soot) was detected in particles in the city center by Kontozova-Deutsch et al. (2011). Granada has a near-continental climate with cool winters, hot summers, and high diurnal temperature variability. Most rainfall occurs during winter and spring seasons, leading to re-suspension of dust particles predominantly in the dry seasons. The average annual precipitation in the area during the test was 427 L m^{-2}. When the wind direction is southerly (S and SW are the prevailing wind directions) marine particles can be expected. Additionally meteorological conditions prevailing in spring and summer favors the arrival of Saharan and Sahel air masses. During autumn and winter the number of Saharan dust episodes is reduced while Atlantic and continental air masses are dominant (Lyamani et al., 2004, 2008, 2010). Regarding atmospheric pollutants, the European legal limits for SO_2, CO, and NO_2 emissions were not surpassed during the test in clear contrast to the O_3, PM10 (particulate matter with an aerodynamic size ca. 10 μm) and soot particles emissions, particularly the latter two (Lyamani and Bravo Aranda, 2009, 2010).

For the two-year exposure test, porous limestone tablets of $10 \times 10 \times 2$ cm (cut from the same limestone slab) were placed vertically at four different sites in the city of Granada (see Fig. 1 for sample location and Table 1 for details). The selected site locations ensure a representative spectrum of microclimatic conditions and thus stone weathering environments ranging from very high (site 4), to high (site 1) and to low polluted areas (sites 2 and 3), as inferred from proximity to heavy traffic streets and data monitored through several stations placed in the city (Fig. 1). Outdoor- and indoor-looking stone faces (here named 'front face' and 'back face' respectively) were distinguished for each site. Comparatively the back faces were more sheltered from rain-wash and sunlight than the front faces. In this work the term "black soiling" always refers to blackening of stones

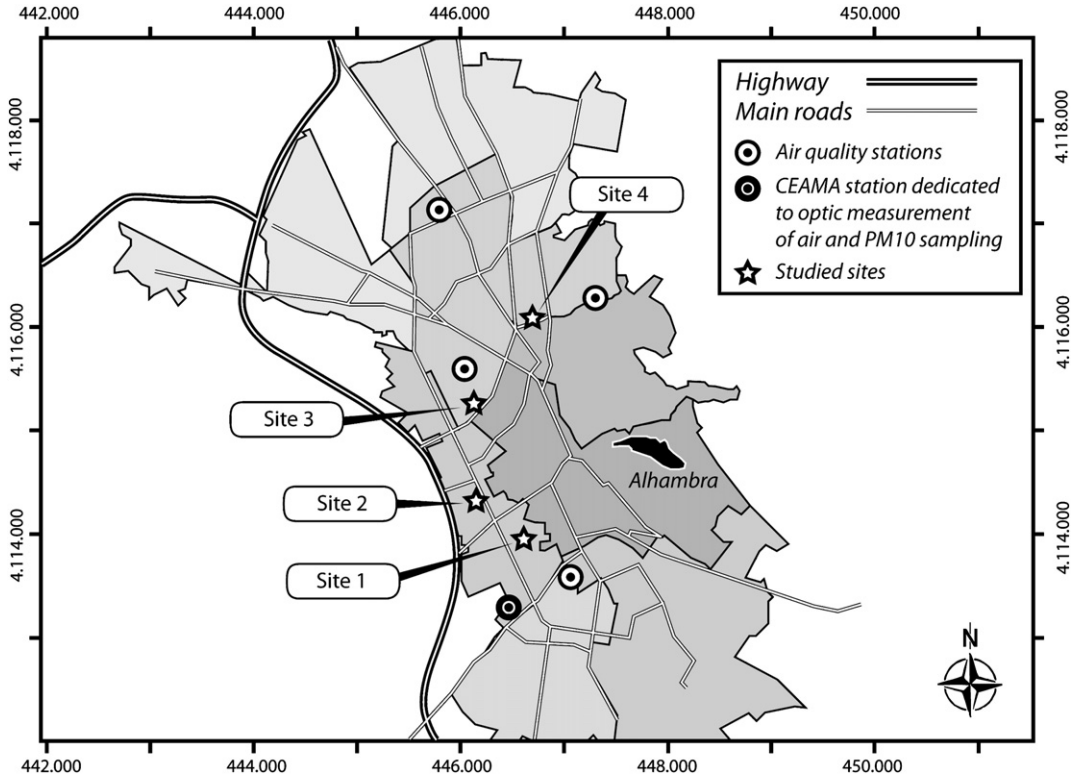

Fig. 1. Location of the sites where porous limestone tablets were placed for the two-year term aging test (stars) in Granada (Spain). Several suburbs of Granada are depicted in gray scale. Highways and main roads are also shown. Location of air quality stations (dotted circle) and particulate matter sampling (CEAMA station, black dotted circle) are shown.

(Grossi et al., 2003) and was related to chromatic changes of lightness or luminosity (L^*) on stone surfaces. The discussion of the results was done considering the impact of atmospheric particles on the porous limestone surfaces and taking into account their exposure conditions (sheltered and unsheltered from rain-wash). However we are aware that soiling also depends on other factors, among which surface roughness, humidity and irradiation are under investigation. Moreover, during the period of stone exposure, PM10 filters were collected at the roof of the Andalusian Center for Environmental Studies (CEAMA), located in Granada (Fig. 1), and analyzed.

2.3. Analytical techniques

Chromatic changes in the limestone tablets were measured with a Minolta CM-700 d spectrophotometer using an 8 mm measuring aperture. The measurements were performed on a regular grid consisting of 18 or 24 points on both back and front faces for each stone tablet. The standard daylight illuminant D65 (color temperature: 6504 K), was applied. The CIE 1976 chromatic scale was used to measure the chromatic parameters L^*, a^* and b^* (Wyszecki and Stiles, 1982). L^* is luminosity or lightness which varies from black with a value of 0 to white with a value of 100; a* varies from +a* (red) to −a* (green) and b* ranges from +b* (yellow) to −b* (blue).

Table 1
Location and description of sites where porous limestone tablets were placed in the city of Granada.

Site location	Exposure conditions	Orientation	Exposure days
1	Unroofed balcony at ~20 m from ground level (g.l.). High traffic density, next to metropolitan works.	ENE	673
2	Roofed balcony at ~7 m g.l. Medium traffic.	NNE	587
3	Unsheltered roof at ~18 m g.l. Medium traffic.	SSE	700
4	Window embrasure at ~2 m g.l. Very high traffic density in narrow and steep street.	S	825

Chip samples of fresh and aged porous limestone tablets were analyzed with an environmental scanning microscope (ESEM). A Phillips Quanta 400 was used applying 20 kV acceleration voltage, 1 nA probe current and working distance of 10 mm. In addition, carbon coated polished thin sections (prepared from aged stone tablets) were studied with a LEO 1430VP scanning electron microscope (VPSEM), coupled with an EDX microanalyzer (Inca 350 version 17, Oxford Instruments). Pinpoint analyses were done using a 500 pA filament current and 10 eV/ch resolution, while working conditions for acquiring X-ray maps were 1 nA filament current and 20 eV/ch resolution. The high-resolution X-ray maps (1024×768 pixels) were obtained in selected areas with 500 frames acquired over 16 h. Furthermore, the *Phasemap* tool implemented in the INCA 350 version was applied to identify mineral phases using ternary element plots of specific pixel information from montaged X-ray maps (Cardell et al., 2009a,b).

The composition and morphology of the atmospheric particles deposited on the stone surfaces and those collected by filters were studied at nanoscale by transmission electron microscopy (TEM). A Philips CM20 equipped with an EDAX solid-state ultrathin-window energy dispersive X-ray (EDX) detector was used. The acceleration voltage of the microscope was 200 kV, and a lens aperture of 40 μm was employed as a compromise between amplitude and phase contrast for the images. The identification of mineral phases was facilitated by collecting selected area electron diffraction (SAED) patterns. Prior to TEM analysis, particles were dispersed in ethanol, sonicated for 30 s, and placed on Formvar© and C-coated Cu grids.

Micro-Raman spectroscopy was applied to distinguish tiny crystals precipitated onto the porous limestone tablets. A Renishaw RM1000 dispersive spectrometer equipped with a Leica DMLM optical microscope, a grating with 1200 grooves/mm and a Peltier-cooled CCD detector were used. Raman spectra were obtained with the 785 nm emission of a diode laser with 30 mW laser power. Leica 20× and 50× objectives were employed. The system was operated

in the confocal mode, resulting in an approximate lateral resolution of ca. 3 μm.

3. Results and discussion

3.1. Characterization of fresh porous limestone surface

At the surface, the *Escúzar* porous limestone is very heterogeneous in texture and composed by micritic calcite (ca. 3–5 μm in size) showing large cavities of ca. 100–300 μm in length, which can be up to 1 cm in length. The larger cavities are covered by sparry calcite (ca. 20–40 μm) and often Fe-rich framboids and Fe-rich tubes occur. Fe-rich framboids comprise small spherules (with diameters of 1–2 μm) forming aggregates of 5–15 μm in length as shown in Fig. 2a. The framboids are mainly composed of Fe and Si, and Al in minor proportions; S is scarce and not always present (see spectrum in Fig. 2a). Based on the Fe-rich framboids morphology and their location in the larger cavities, we suggest that they can be oxyhydroxides

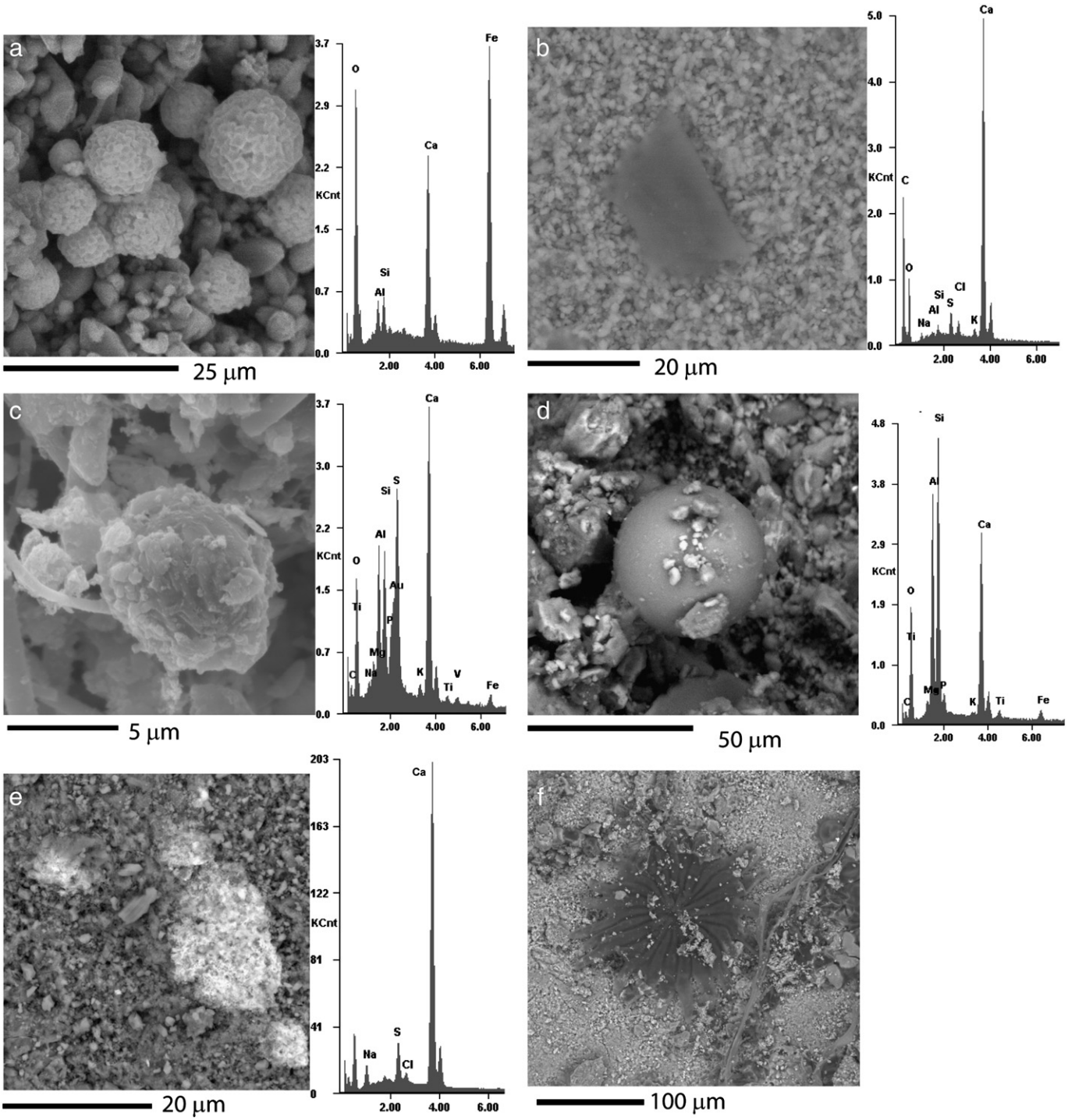

Fig. 2. Representative SEM images and corresponding SEM-EDX spectra of Escúzar porous limestone and particulate matter filters. (a) Aggregate of several Fe-rich framboids on fresh (quarried) stone sample. (b) C-rich particle mixed with clay minerals and phyllosilicates, NaCl and Ca-sulfate on stone tablet at site 4. (c) Phyllosilicates and clay minerals mixed with Ca-sulfate and traces of V and Ti in PM10 filter. (d) Si–Al-rich spherical particle on stone tablet at site 1. (e) Porous aggregate of sea-salt particles (NaCl) mixed with Ca-sulfate on stone tablet at site 2. (f) Biogenic particle (Leaf Trichome) in the center and fungal hyphaea (right) on stone tablet at site 1.

pseudomorphs of former framboidal pyrites originated by oxidation and sulfur loss during early stages of diagenesis (e.g. Merinero et al., 2009). Fe-rich tubes are likewise interpreted. Additionally the fresh stones may contain clay minerals (hydrous aluminum phyllosilicates with particle size <2 μm) and occasionally sphalerite (Zn,Fe)S.

3.2. Atmospheric particles deposited on the porous limestone tablets and filters

In the following paragraphs a simple classification of the identified atmospheric particles deposited on the aged porous limestone surfaces and the PM10 filters collected at the CEAMA station is presented (Table 2). However it is worth noting that complex mixtures between these groups are very common.

3.2.1. Soil dust particles

Phyllosilicates (parallel sheets of silicate tetrahedra with Si_2O_5 or a 2:5 ratio) with sizes commonly ranging from 40 to 100 μm, and clay minerals are by far the most common particles found in all sites (Table 2). These particles have both primary and secondary (airborne) origins. Although pure phyllosilicates and clay minerals were observed (probably those corresponding to a primary origin), most commonly they form complex mixtures with other atmospheric particles. For example, Fig. 2b shows a C-rich particle mixed with NaCl and Ca-sulfate and phyllosilicate particles. This mixture also was observed in the filters, possible indicating an airborne origin of the phyllosilicates (Fig. 2c). At nanoscale (e.g. Fig. 3a) the mixture is more obvious, including variable amounts of C, Cl, Ca-sulfate and CaMg-sulfate and occasionally NaCl. Based on the chemical composition, the observed clay minerals comprise illite $(K,H_3O)(Al,Mg,Fe)_2(Si,Al)_4O_{10}[(OH)_2,(H_2O)]$, paragonite $NaAl_2(Si_3Al)O_{10}(OH)_2$, smectite $(Na,Ca)(Al,Mg)_6(Si_4O_{10})_3(OH)_6{-}nH_20$, kaolinite $Al_2Si_2O_5(OH)_4$ and chlorite $(Mg,Fe)_3(Si,Al)_4O_{10}(OH)_2\cdot(Mg,Fe)_3(OH)_6$, as reported elsewhere for the city of Granada (Rodríguez-Navarro and Sebastián, 1996; Kontozova-Deutsch et al., 2011).

Table 2
Summary of the identified atmospheric particles by SEM-EDX and TEM on the studied limestone tablets at the different sites and the filters collected at the CEAMA station in the city of Granada (Southern Spain).

	Fresh	Site 1	Site 2	Site 3	Site 4	Filter
Fe-rich framboids	●	●	●	○	●	○
Fe-rich tubes	●	●	○	○	●	○
Atmospheric particles						
Dust particles (phyllosilicates and clay minerals)	●	●	●	●	●	●
Fly ash particles (Si–Al-rich)	○	●	●	○	●	○
Fe-rich particles	○	○	○	○	●	○
Soot particles (C-rich)	○	●	●	●	●	●
Salt particles	○	○	●	○	○	○
Other particles						
Dolomite	○	●	●	○	●	●
Calcite	●	●	●	●	●	●
Fe–Ti-oxide	○	○	●	○	○	○
Fe-oxide	○	●	●	○	○	○
Sphalerite	○	○	●	○	○	○
Barite	○	○	●	○	○	●
Feldspar	○	○	●	○	●	○
Chalcopyrite	○	●	○	○	○	○
Rutile	○	○	○	○	○	●
Quartz	○	○	○	○	●	○
Biogenic particles						
Fungal hyphae	○	●	●	●	●	○
Leaf Trichome	○	●	●	○	●	○
Black gypsum crust	○	●	○	●	●	○

● Observed ○ not observed.

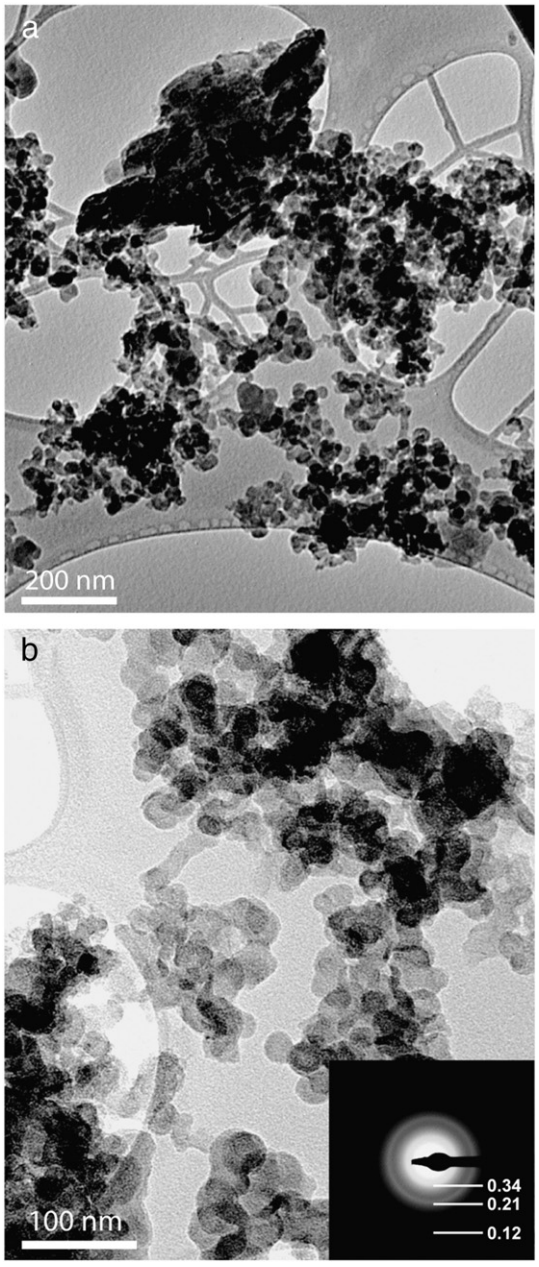

Fig. 3. Examples of particulate matter (PM10) on filter. (a) Clay minerals mixed with Ca-sulfate (upper left) and soot with fractal geometry. (b) Detail of soot particles composed of irregular C-rich spherules leading to high porous aggregates. Inset: SAED pattern showing graphitic carbon reflections corresponding to carbon-layer spacings.

3.2.2. Fly ash particles

These silicon- and aluminum-rich particles are perfectly spherical with smooth surface (Fig. 2d). They contain minor amounts of Mg, Fe, Ti, K, S and occasionally Cl, showing a wide range in size that goes from 2 to 40 μm. Similar particles have been observed elsewhere and are commonly interpreted as derived from coal combustion (Kindratenko et al., 1994; Xie et al., 1994; Katrinak et al., 1995; Rodríguez-Navarro and Sebastián, 1996; Esbert et al., 2001; Kontozova-Deutsch et al., 2011).

3.2.3. Iron-rich particles

These particles are generally rounded in shape and can be related to diesel exhaust, mainly composed of soot and metallic particles bearing Fe and Fe–S as major elements. Metal-rich particles are important in the development of black crust since they usually contain

several metals such as V, Co, Ni, Cu, Mn and Cr that, together with carbonaceous particles, catalyze the oxidation and hydrolysis of atmospheric SO_2 (Rodríguez-Navarro and Sebastián, 1996 and references therein).

3.2.4. Soot particles

These carbon-rich particles were observed on all stones, usually mixed with clay minerals. C-rich particles with detectable amounts of Na, K and Cl also were observed by means of SEM-EDX analyses and more precisely by TEM. These particles are comprised of both organic matter (made up of hundreds of individual carbon compounds) and elemental carbon (soot) forming the fine and ultrafine particulate matter fraction (e.g. Esbert et al., 2001; Murr and Bang, 2003). TEM observations of particles collected from the filters revealed the widespread occurrence of soot particles (Fig. 3a and b) with fractal geometries, i.e. concentric graphene-like layers, which are wrapped into spherules that aggregate into characteristic branching clusters of hundreds of carbonaceous spherules (e.g. Katrinak et al., 1995; Pósfai et al., 1999; Murr and Bang, 2003; Simão et al., 2006; Pósfai and Buseck, 2010). Individual carbonaceous spherules range in size from 20 to 60 nm with an average value of 32 ± 11 nm, matching those observed from diesel particulate matter (Simão et al., 2006). The SAED patterns are dominated by diffuse (non-crystalline) carbon reflections although occasionally diffuse rings at 0.12, 0.21 and 0.34 nm (Fig. 3b inset) indicate the occurrence of graphite (Murr and Bang, 2003; Simão et al., 2006). Micro-Raman analyses further confirmed the occurrence of soot as revealed by the two broad bands around 1300 and 1600 cm^{-1} attributed to the D (disordered) and G (graphitic) bands typical of soot particles (Fig. 4). Additionally, the high luminescence of the Raman spectrum also suggests the occurrence of organic matter or organic carbon.

3.2.5. Salt particles

Highly porous Na and Cl rich particles (up to 20 μm in length) were occasionally observed (Fig. 2e). These particles have compositions similar to aged sea salts and are characterized by a decrease in the ratio Cl/S due to particle modification during long-term transport in the atmosphere (Esbert et al., 2001). It is worth noting that sea salt particles are reported in other near-continental areas of Spain (e.g. Querol et al., 2004) including the city of Granada (Kontozova-Deutsch et al., 2011; Horemans et al., 2011).

3.2.6. Other particles

Under this category a wide spectrum of observed mineral dust particles are classified, including dolomite ($CaMg(CO_3)$) and fibrous calcite ($CaCO_3$), barite ($BaSO_4$), Fe-oxides, sphalerite, Fe–Ti particles (ilmenite and/or rutile, TiO_2), chalcopyrite ($CuFeS_2$), feldspar $(Na/K/Ca)Al_{(1-2)}Si_{(3-2)}O_8$, and quartz Si_2O.

3.2.7. Biogenic particles

Evidence of biological colonization was found on stones located at all sites mainly in the form of lichens and fungal hyphae, the latter showing elongated structures ca. 50 mm wide by more than 500 μm long (Fig. 2f) as observed Viles and Gorbushina (2003) for a similar period of time. The widespread occurrence (Table 2) of radial and starry shape organic structures (200 μm in length), tentatively classified here as *olive leaf trichome* (e.g. Filippou et al., 2007), also should be noted.

3.3. Black soiling

After two years of exposure to the Granada urban air, macroscopic changes on both the front and back faces of almost all porous limestone surfaces were evident, namely color modification and darkening, edge-rounding of the stone tablets and organic colonization (see above). As an example, Fig. 5 shows the surface modification of the limestone tablet placed at site 1 (high polluted area) after two years of urban exposure. Surface roughness was higher in the front face (Fig. 5a) than in the back face (Fig. 5b), which is attributed to the more intense rain wash-out of the front stone side, further promoting differential erosion between micritic and sparitic calcite (with crystal sizes <4 μm and >10 μm respectively) areas (Vendrell et al., 1996; Viles, 2005). Additionally it should be noted that rain-sheltered areas are more suitable for gypsum crust development which in turn may explain smooth surfaces (Delalieux et al., 2002).

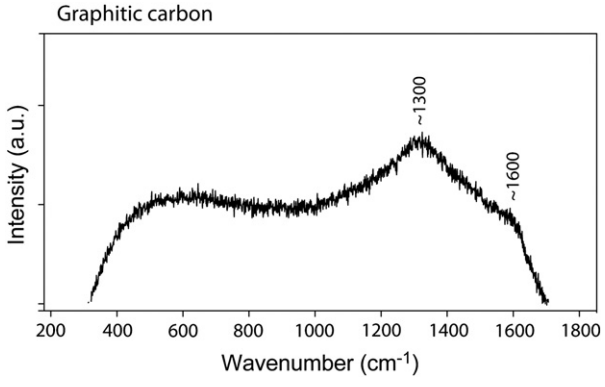

Fig. 4. Example of Raman spectrum of black particles deposited on porous limestone surface. Note the broad bands around 1300 and 1600 cm^{-1} attributed to the D (disordered) and G (graphitic) bands respectively, indicating graphitic carbon derived from atmospheric soot particles.

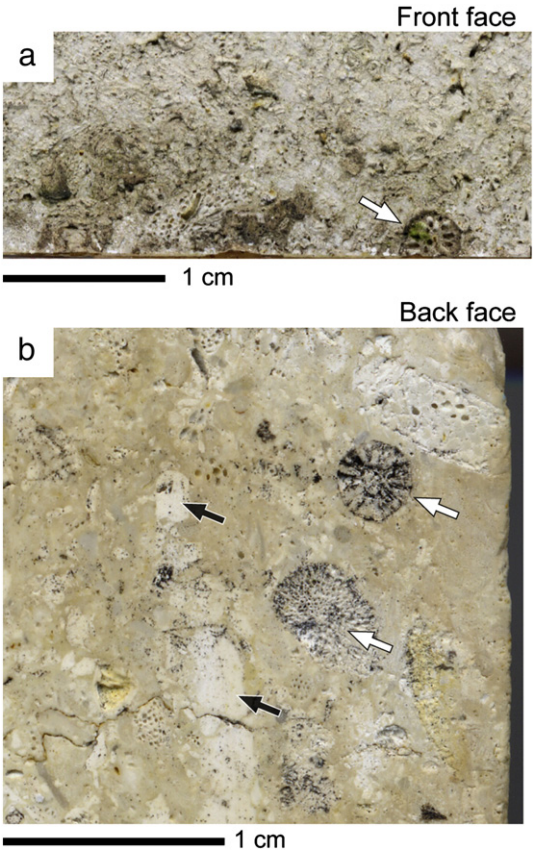

Fig. 5. Scanned surface of porous limestone tablet place at site 1 after the on-site two-year term test. (a) Front face; note the surface roughness compared to the back face. The white arrow shows one bioclast (bryozoan) partially colonized by organic material. (b) Back face; the white arrows indicate two blackened bioclasts (bryozoans). Other bioclasts (e.g. red algae, black arrows) are less or not blackened.

In the stone surface blackening was heterogeneous at the centimeter scale, and more obvious in certain types of bioclasts displaying abundant intraclast porosity, such as bryozoans (Fig. 5b).

In order to assess the soiling process chromatic changes on the front and back stone faces were measured using spectrophotometry. Table 3 shows mean values and standard deviations of L^*, a^*, b^* and C^* for the *Escúzar* porous limestone. Black soiling can be estimated by measuring the decrease in L^* at a certain time (L_t^*) with respect to the initial conditions L_0^*, namely final soiling, $\Delta L^* = L_t^* - L_0^*$ (e.g. Grossi et al., 2003). Table 3 displays absolute ΔL^* between fresh and aged limestone tablets for the period of time investigated, indicating a decrease in lightness (i.e. blackening) on both the back and front stone faces at all sites (Table 3). Black soiling was particularly evident at site 4 ($\Delta L^* = -10.84$ on front face and -11.53 on back face) and site 1 ($\Delta L^* = -8.12$ vs. -5.97 units for front and back faces respectively) which correspond to the most polluted areas (see Table 1). Moreover, Table 3 reveals a statistically significant increase in the chromatic parameters a^* and b^* on all studied porous limestone tablets (on both back and front faces), which results in a displacement toward more red and yellow tonalities (i.e. warmer colors) of the stones.

In order to better appreciate the effect of black soiling on the *Escúzar* porous limestone, the L^*, a^*, b^* and C^* values were plotted as shown in Fig. 6. The degree of chromatic modification can be estimated by comparing the scatter of the data between the fresh tablet and the aged stone tablets. Fig. 6a shows that parameters a^* and b^* were modified to some extend in the front faces particularly on stones placed at sites 1 and 4, where differences of up to 3 and 10 units for a^* and b^* respectively were found. For the back faces (Fig. 6b) data were more scattered though again limestone located at the most polluted areas (sites 1 and 4) showed the highest tonality changes compared to the fresh stone tablet.

Variations in lightness (L^*) relative to chroma (C^*) are displayed in Fig. 6c and d, where a negative correlation can be seen indicating a black soiling process (soiling tends to increase C^*, i.e. color intensity, when L^* decreases). Once again results show that stone soiling was more acute in sites 1 and 4 (polluted areas) in both the front and back stone faces, though data were more scattered in the back stone faces (Fig. 6d). As previously noted the scattering of the chromatic data can be related to a differential erosion process of the stone related to the porous limestone heterogeneous texture (uneven distribution of micritic matrix and diverse types of bioclasts–sparitic areas; see Fig. 5a and b). However, as mentioned before, surface roughness on front stone surfaces is more flat than on the back faces, which might favor less scattered chromatic data.

Lightness (ΔL^*) and chroma (ΔC^*) absolute differences for all aged limestone tablets (on both front and back faces) were plotted with respect to the fresh quarried stone tablet as Fig. 7 exhibits. In the CIELAB color space a color change – perceptible to the human eye – is defined by lightness and chroma differences greater than 3 units (Völz, 2001). In this work a perceptible darkening was observed on both the front and back faces of all stones, except on the back face of porous limestone placed at site 2 (Fig. 7a). Regarding chroma variations, only visual changes were noticed on stones placed in the most polluted sites ($\Delta C^* > 3$) and with little difference between the front and back faces (Fig. 7b).

On the other hand, the area of a stone surface covered by atmospheric particles (i.e. effective area coverage, EAC) can be estimated from the following expression (Pio et al., 1998; Grossi et al., 2003):

$$\frac{L_t^*}{L_0^*} = (1 - AC) + \frac{L_p^*}{L_0^*} AC \quad (1)$$

where AC is the area fraction covered by particles and L_p^* is the lightness of the settled particles (which here is assumed to be 30 for simplicity, Grossi et al., 2003). Table 4 shows the estimated EAC values ($EAC = 100 \cdot AC$) for the front and back faces of all tested stones. Those stones placed next to dense traffic streets (sites 1 and 4) exhibited the highest EAC values on both the front and back faces (ranging from 10.2% to 20.4%) compared to stones located at lower polluted areas with EAC values ranging from 1.7 to 9.4%. It is considered that EAC values above 2% are perceptible for the human eye and values up to 5% would trigger public complaints (in Grossi et al., 2003). These limit values, however, have to be taken with care as human perceptibility also depend of the overall lightness of surrounding buildings. In this work, all stone surfaces (rain-sheltered and unsheltered) exposed to the urban environment of Granada in a two years time span (except one) have surpassed this value.

The soiling coefficient (capacity of soiling of a stone independently of time and total suspended particulate, TSP, concentration) of building stone surfaces can be further determined by measuring changes in reflectance (lightness) through time when the concentration of the blackening agent in the air is known (e.g. Pio et al., 1998; Grossi et al., 2003; Brimblecombe and Grossi, 2004, 2009). Several equations have been proposed to describe the soiling of building materials, namely linear, simple or bounded exponential, power and square-root fitting (see Brimblecombe and Grossi, 2004 for a comprehensive review). In the past, the most popular model applied to soiling data was the square-root fitting that seems to be appropriate for relatively short periods of time such as used in this study and can explain the rate of the initial soiling. In this way, the change in reflectance at a certain time is linearly related to the square root of time (t) and the amount of TSP by the following expression,

$$L_t^* = L_0^* - SC_r \sqrt{TSP \cdot t}, \quad (2)$$

where SC_r is the soiling coefficient for a square-root fitting model. Grossi et al. (2003) found that each stone has a characteristic SC_r

Table 3
Lightness (L*), a* and b* parameters and chroma ($C^* = \sqrt{(a^*)^2 + (b^*)^2}$) for fresh and aged tablets of porous limestone after exposure to urban environment in several sites of Granada (see Fig. 1 and Table 1 for locations). ΔL^* and ΔC^* mean difference in lightness and chroma with respect to the fresh quarried limestone sample.

	n	L*	σ	a*	σ	b*	σ	C*	σ	ΔL*	ΔC*
Front face											
Fresh	24	91.00	0.56	0.34	0.17	5.90	0.40	5.91	0.40		
Site1	24	82.89	2.10	1.57	0.23	9.79	1.19	9.91	1.21	−8.12	4.00
Site2	18	87.00	0.59	0.67	0.07	7.39	0.58	7.42	0.58	−4.01	1.51
Site3	22	86.34	1.47	0.66	0.12	6.39	0.74	6.42	0.74	−4.66	0.51**
Site4	20	80.16	5.93	1.41	0.96	10.13	3.79	10.24	3.89	−10.84	4.33
Back face											
Fresh	24	90.86	0.81	0.55	0.12	7.48	0.92	7.50	0.92		
Site1	24	84.89	2.83	1.05	0.38	11.44	3.39	11.49	3.41	−5.97	4.00
Site2	22	89.81	0.78	0.52	0.14	6.80	0.58	6.82	0.59	−1.05	−0.67**
Site3	22	85.33	1.46	0.78	0.07	6.99	0.76	7.03	0.76	−5.53	−0.47**
Site4	24	79.33	5.24	1.47	0.82	11.20	3.24	11.30	3.32	−11.53	3.81

n = number of measurements, σ = standard deviation. All differences are statistically significant at P = 0.01 except for those marked with two asterisks.

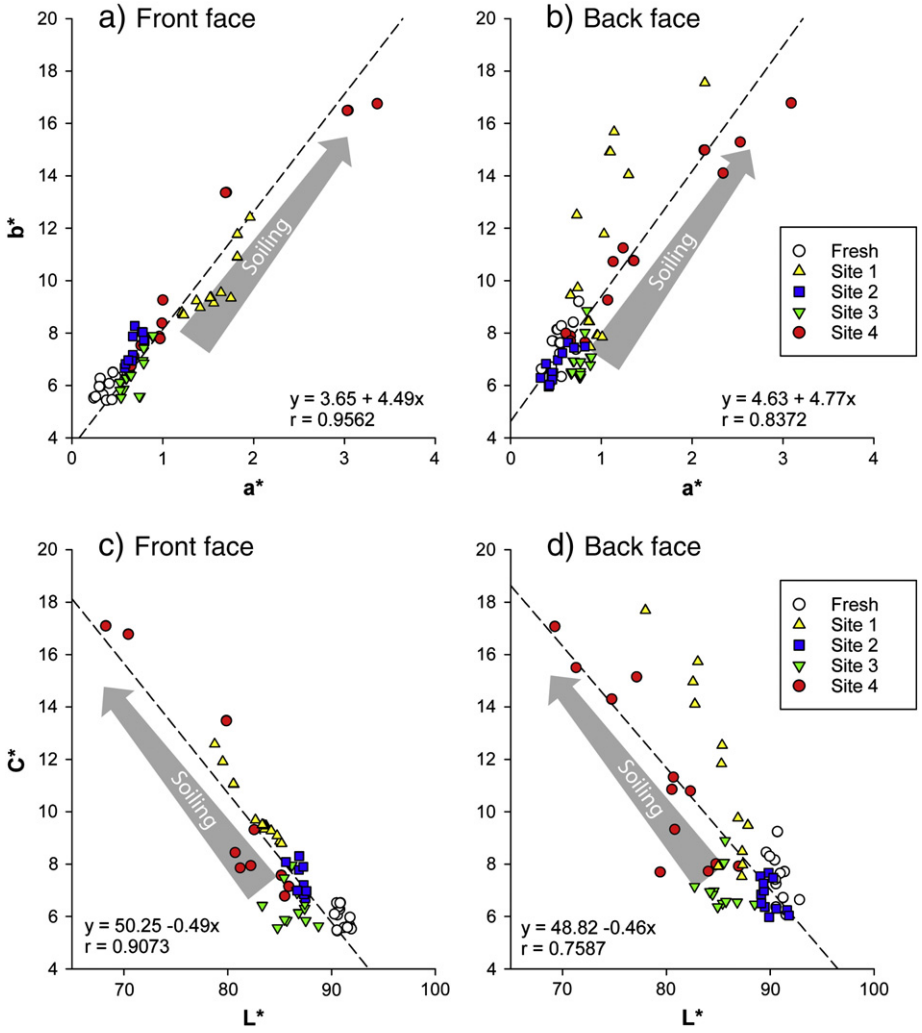

Fig. 6. Variations in the absolute chromatic values a* relative to b* components in (a) front faces and (b) back faces for different locations exposed at the urban Granada conditions. Initial values are those corresponding to the quarried stone slab (empty dots). Variations in lightness (L^*) relative to chroma (C^*) in (c) front faces and (d) back faces. Dashed lines are linear fits to the data. Fit equation and correlation coefficients are shown in each figure.

and that mainly depends on the initial stone lightness L_0^* (SC_r is higher when L_0^* is higher). Therefore, high SC_r values indicate that the blackening rate (negative changes in ΔL^* through time) of the stone surface is very high at constant TSP concentration. For longer periods of time, the bounded exponential model provides, however, a more physically realistic model to describe the soiling process (Brimblecombe and Grossi, 2004, 2009). In this case the equation describing the soiling is,

$$L_t^* = (L_0^* - L_\infty^*) \cdot \exp(-SC_e \cdot TSP \cdot t) + L_\infty^* \quad (3)$$

where L_∞^* is the lightness after infinite soiling. The most difficult parameter to constrain in Eqs. (2) and (3) is TSP, and even more challenging is to estimate the proportion of TSP responsible for blackening which is commonly associated to elemental carbon or black carbon (Pio et al., 1998; Grossi et al., 2003; Grossi and Brimblecombe, 2004; Brimblecombe, 2011). In our study the mean PM10 concentrations (Lyamani and Bravo Aranda, 2009, 2010) measured during atmospheric aerosols campaigns conducted in the city of Granada between 2008 and 2009 were used as a first proxy for estimating SC_r and SC_e of the closest locations (see Fig. 1 for location of air quality stations). In these air quality stations black carbon particles were not directly measured but inferred from absorbing aerosols (Lyamani and Bravo Aranda, 2009, 2010). Additionally, it was also difficult to constrain the lightness after infinite soiling (L_∞^*) in Eq. (3) for the studied porous limestone because of the lacking of reliable data in the literature. It is worth to mention that, although this type of porous limestone has been used in the past (e.g. Granada's Cathedral, Rodriguez-Navarro, 1994), its use as a restoration stone dates since the last decade. However some assumption can be made in order to constrain this value. Based on extensive blackening data, Brimblecombe and Grossi (2009) argued that L_∞^* depends on the elemental carbon (EC) concentration in the atmosphere. Reductions of 75–80%, 60–70% and 30–40% of the original lightness was found in remote areas (EC<1 μg m^{-3}), urban background sites (EC~2–3 μg m^{-3}) and highly traffic areas (EC>10 μg m^{-3}). Surface concentration of EC is also useful when an estimation of L_∞^* is required but unfortunately the previous studies of black crusts in the city of Granada do not provide this data (e.g. Rodríguez-Navarro and Sebastian Pardo, 1996).

However, even though no systematic data of EC in the atmosphere at different sites in the city of Granada are available, it is clear the high proportion of black particles in the particulate matter. For instance, Kontozova-Deutsch et al. (2011) reported that ca. 9% of black carbon particles (soot particles) were present in collected bulk particulate matter from the outer part of the monastery of San Jerónimo located close to a traffic street in Granada. Based on light scattering and absorption properties of aerosol particles in Granada, Lyamani et al. (2008) found seasonal and diurnal variations of the single scattering albedo at 670 nm (ω_{0A}) indicating fluctuations in the proportion of

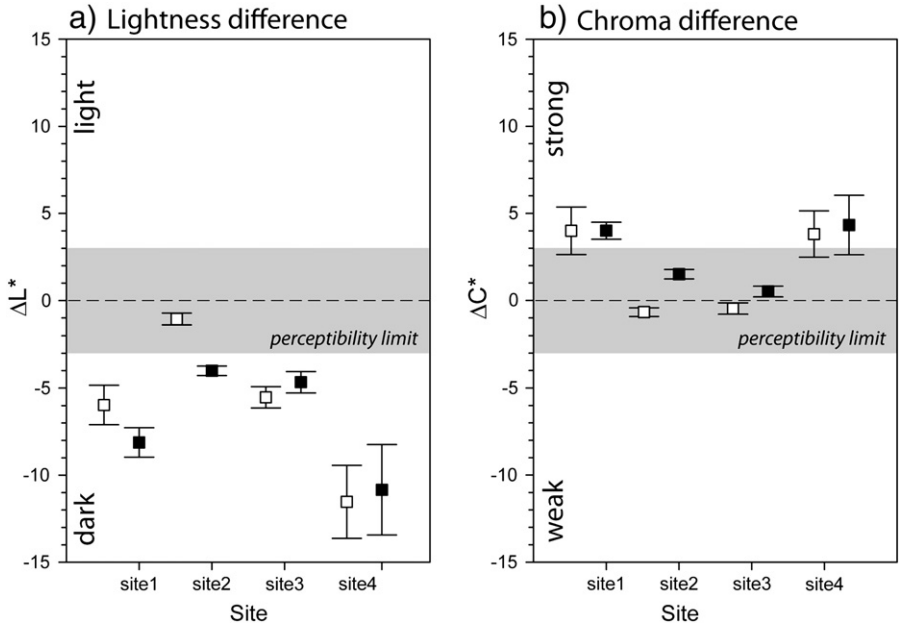

Fig. 7. (a) Lightness and (b) chroma absolute differences with respect to the fresh quarried porous limestone slab. Empty and filled symbols are back and front faces respectively. Squares are mean values and bars are the confidence intervals for the mean at 95%. Data outside the gray area (absolute change greater than ±3 units) are considered to be perceptible.

purely scattering aerosols (e.g. sulfates, where $\omega_{0A}=1$) and strongly absorbing aerosols (e.g., to black carbon, $\omega_{0A}=0$). Median values of single scattering albedo ω_{0A} ranged from 0.6 (winter) to 0.8 (summer) measured in the CEAMA station in the city of Granada (Fig. 1), with average values ranging from 0.5 to 0.8 (median annual values gathered around 0.7). These average values can be considered as a first approximation of the expected final reflectance or lightness if removal processes are discarded. Therefore, based on albedo measurements in Granada, (Lyamani et al., 2008), we estimate that $L_\infty{}^*$ would represent the 85–55% of the original lightness in agreement with the results of Brimblecombe and Grossi (2009) for remote areas and urban background sites (see above). On the other hand, Querol et al. (2004) observed that EC and organic carbon concentrations in Spain accounted for 10–25% (2.5–4.5 $\mu g\cdot m^{-3}$) of the regional PM10, 35% (~5 $\mu g\cdot m^{-3}$) of the urban background and 43% (~4 $\mu g\cdot m^{-3}$) of the urban curbside site levels from Mediterranean and Atlantic regions. Only very recently Horemans et al. (2011) provided data of direct measurements of black carbon (BC) concentration for indoor and outdoor conditions in the Alhambra monument and two nearby streets (Horemans et al., 2011). Background values show daily black carbon fluctuation ranging from 0 $\mu g\cdot m^{-3}$ to 15 $\mu g\cdot m^{-3}$ with an average of 2 $\mu g\cdot m^{-3}$ (Horemans et al., 2011). Curbside values are, however, much higher, ranging from 1 to 15 $\mu g\cdot m^{-3}$ and average of 8 $\mu g\cdot m^{-3}$. If these values are considered as representative for the city of Granada, BC in urban backgrounds and traffic areas would represent ca. 14% and 37% of PM10 respectively. These proportions were used to estimate a rough value of BC concentration in the four sites studied in this work (Table 4).

Table 4 shows the values of SC_r for the front and back faces of all sites. Two values of soiling coefficients (based on PM10 concentration and estimated BC concentration) for each site are given. SC_t based on PM10 values for the front faces ranged from 2.8 to 6.0×10^{-2} $days^{-1/2}\,\mu g^{-1/2}\,m^{3/2}$ (higher in polluted sites) whereas on back faces the range was wider (0.7 to 6.4×10^{-2} $days^{-1/2}\,\mu g^{-1/2}\,m^{3/2}$). These values are comparable to

Table 4
Relative lightness difference (ΔL*), effective area coverage (EAC), time of exposure under urban conditions (t), particulate matter less than 10 μm (PM10), estimated BC concentration and estimated soiling coefficient based on root-square (SC_r) and bounded exponential fitting (SC_e) for the front and back stone faces from the studied sites using PM10 and BC concentration.

	ΔL* (%)	EAC (%)	t (days)	ΔL[a] per day (day^{-1})	ΔL[a] per year ($year^{-1}$)	PM10[a] ($\mu g\cdot m^{-3}$)	BC[b] ($\mu g\cdot m^{-3}$)	$SC_r\times10^{-2}$ (PM10) ($days^{-1/2}\,\mu g^{-1/2}\,m^{3/2}$)	$SC_r\times10^{-3}$ (BC) ($days^{-1/2}\,\mu g^{-1/2}\,m^{3/2}$)		$SC_e\times10^{-4c}$ (BC) ($days^{-1}\,\mu g^{-1}\,m^3$)
Front face											
Site1	−8.9	14.0	673	−0.013	−4.8	41	15.17	4.9	8.0	Sites 1 and 4	0.99
Site2	−4.4	6.7	587	−0.008	−2.7	35	4.2	2.8	8.1	Sites 2 and 3	1.43
Site3	−5.1	7.8	700	−0.007	−2.7	40	4.8	2.8	8.0		
Site4	−11.9	19.0	825	−0.014	−5.3	39	14.43	6.0	9.9		
Back face											
Site1	−6.6	10.2	673	−0.010	−3.6	41	15.17	3.6	5.9	Sites 1 and 4	0.92
Site2	−1.2	1.7	587	−0.002	−0.7	35	4.2	0.7	2.1	Sites 2 and 3	1.19
Site3	−6.1	9.4	700	−0.009	−3.2	40	4.8	3.3	9.5		
Site4	−12.7	20.4	825	−0.015	−5.6	39	14.43	6.4	10.6		

[a] Daily mean values for 2009 of closest air quality stations (Lyamani et al., 2008) (cf. Fig. 1 and Table 1).
[b] Based on BC proportions measured by Horemans et al. (2011) in Granada and assuming that sites 1 and 4 represent traffic areas and 2 and 3 are urban backgrounds. See text for details.
[c] Assuming a final lightness of 77 based on albedo measurements (Lyamani et al., 2008) and Brimblecombe and Grossi (2009). See text for details.

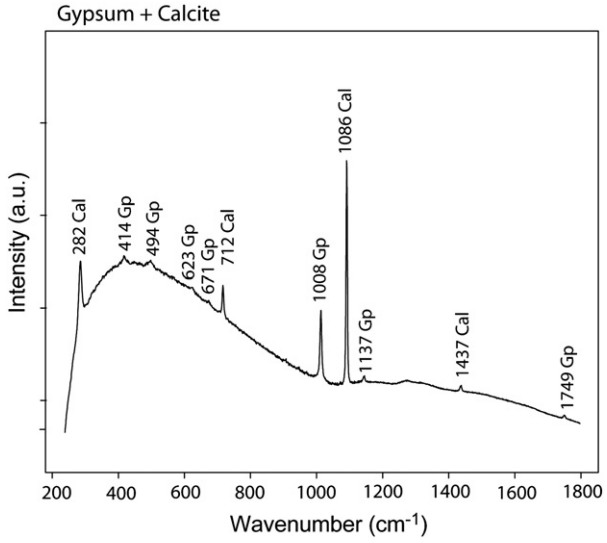

Fig. 8. Raman spectrum of the stone crust showing the occurrence of a mixture of gypsum (Gp) and calcite (Cal).

those values obtained for other types of bioclastic calcarenite placed in urban conditions in Atlantic (from 8.8 to 10.2×10^{-2} days$^{-1/2}$ μg$^{-1/2}$ m$^{3/2}$) and continental climates (from 5.0 to 8.1×10^{-2} days$^{-1/2}$ μg$^{-1/2}$ m$^{3/2}$) (Grossi et al., 2003). Nevertheless this comparison is not straightforward as the later values were obtained for horizontal surfaces and using TSP instead of PM10. Removal processes vary in a different way for horizontal and vertical surfaces resulting in different soiling coefficient values (Grossi et al., 2003; Watt et al., 2009). SC_t values based on estimated BC concentration are startling similar (8.0–9.9×10^{-3} days$^{-1/2}$ μg$^{-1/2}$ m$^{3/2}$) suggesting that the use of BC instead of PM10 concentration is more robust to constrain the soiling coefficient. Furthermore, as Table 4 shows, minor differences in SC_r and SC_t were found between the front and back faces of all stones except for site 2. Considering that the soiling coefficients refer to the soiling capability of a stone and thus are independent of time and TSP concentration, the differences noticed here should be attributed to other factors. As mentioned above, differences in surface roughness between the front and back faces due to different exposure conditions controlling stone differential erosion would play an important role.

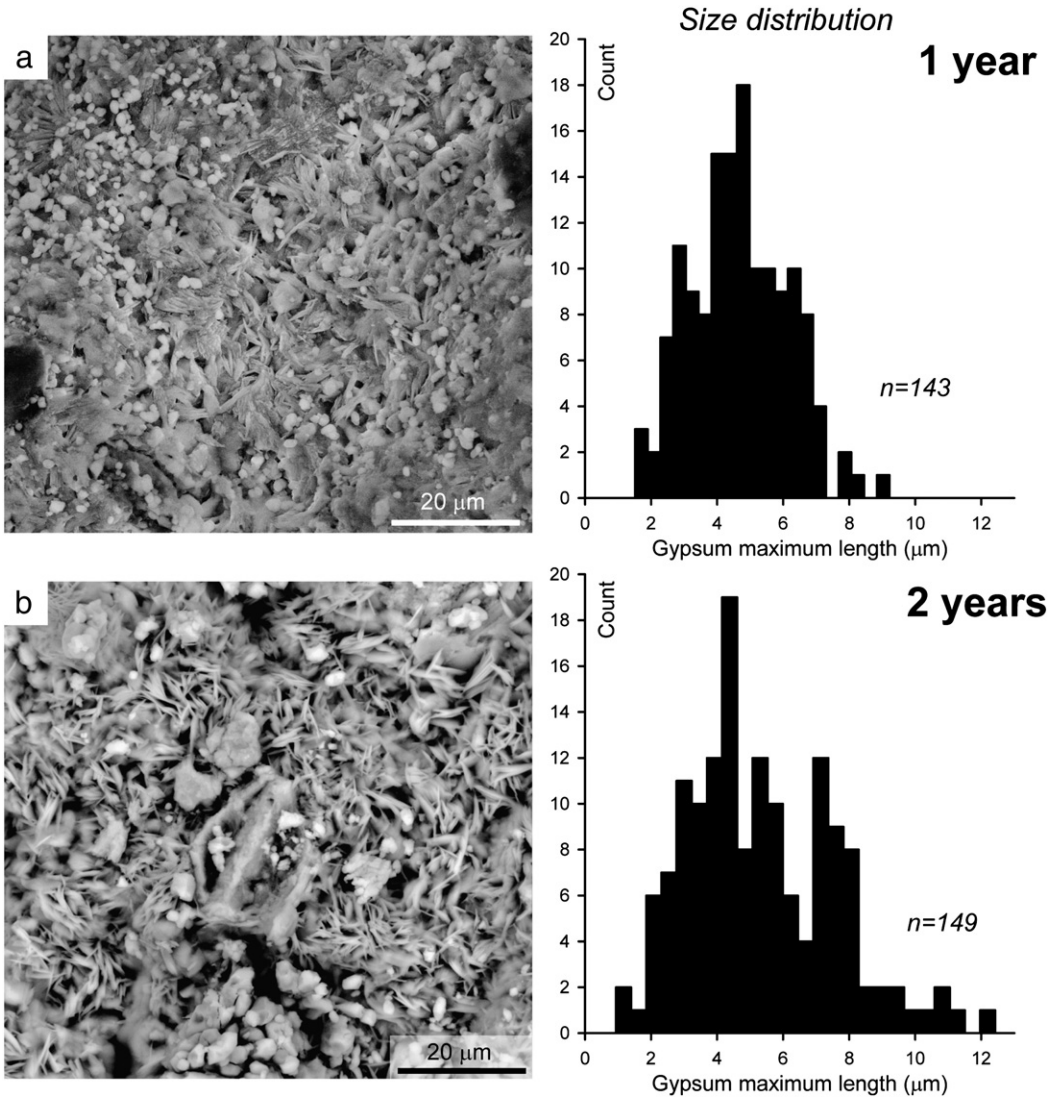

Fig. 9. SEM images showing the gypsum crust formed on the back surface of the porous limestone tablet placed at site 1 (high polluted area) after (a) one year and (b) two years of urban exposure. Note the tabular and more massive gypsum crystals developed after two years of test. Right: histograms obtained by image analysis from the corresponding SEM pictures showing gypsum crystal size distribution.

In order to estimate SC_t, data from sites 1 and 4 were selected as representative of traffic areas and from sites 2 and 3 as urban background (Table 4). It was found that SC_t based on estimated BC concentration, ranged from 0.99 to 1.43×10^{-3} days^{-1} μg^{-1} m^3 for the front stone faces. These values are preferred when estimating changes in stone lightness for extended periods of exposure under urban conditions. Nevertheless care should be taken when using these parameters for shorter period of time (Brimblecombe and Grossi, 2004; Grossi and Brimblecombe, 2008).

3.4. Gypsum crust formation

Gypsum crusts were found in all sites with the exception of site 2. The occurrence of gypsum was confirmed by means of micro-Raman spectroscopy as shown in Fig. 8. SEM observation revealed that gypsum crystals varied from tabular (rose-shape) to more massive morphologies (Fig. 9). Small and euhedral (well-formed crystals) calcite rombohedrons (up to 5 μm) were often seen mantled by the gypsum crust. More likely the occurrence of these euhedral calcite crystals may result from the disintegration of the calcitic matrix, however it cannot be discounted as possibly resulting from dissolution-precipitation processes associated to the gypsum crust formation. Fig. 9 shows two SEM images of the aged stone tablet (back face) placed at site 1 (high polluted area) during the aging test. The gypsum crust was developed after the first year of exposure, with mean value of gypsum crystal sizes of 4.7 ± 1.4 μm (Fig. 9a). After the second year of exposure more abundant and bigger gypsum crystals, up to 12 μm, were formed as observed in Fig. 9b (and corresponding histogram).

At the end of the test the thickness of all gypsum crusts was determined by means of SEM-EDX elemental mapping obtained from thin sections elaborated normal to the aged stones. Fig. 10 shows a false-color mineral map elaborated from a SEM-EDX elemental mapping of the aged porous limestone placed at site 1 (back face). It can be observed that gypsum crust formation is controlled by the surface roughness of the stone, which is ultimately related to the occurrence of bioclasts with intraclastic porosity. Here the thickness of the gypsum crust attained ca. 50 μm (Fig. 10a), though thickness up to ca. 100 μm has been also found. Gypsum crystals also were detected filling limestone pores at depths of ca. 500–700 μm (Fig. 10a and b). Average spectra (Fig. 10a and b) obtained from the gypsum crust indicate the occurrence of Si, Al, K and C suggesting that mineral dust particles and soot particles are mixed with the gypsum in the crust.

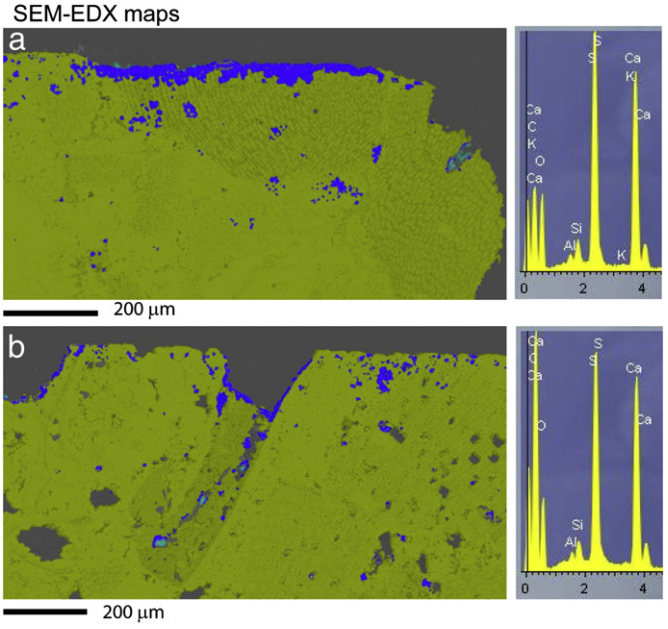

Fig. 10. False-color mineral maps elaborated from SEM-EDX elemental mappings from thin sections cut normal to limestone tablet placed at site 1 (back face). Pistachio represents calcite and blue gypsum. (a) Gypsum crust is preferentially developed over bioclasts. (b) Gypsum crust is irregularly developed on the surface of a large cavity and filling deeper limestone pores. Right: corresponding average spectra of gypsum-rich areas (blue areas).

4. Concluding remarks

In this work the black soiling of the building *Escúzar* porous limestone was estimated after a two-year exposure under different contaminated urban conditions in the city of Granada (Southern Spain). The final goal was to evaluate the Cultural Heritage suitability of this stone to replace similar historic limestones in monuments in Andalusia, and its endurability in present civil buildings. The soiling process was studied by measuring variations in chromatic parameters, particularly in lightness (L^*, whose decrease indicates blackening of stones) on the front (rain-unsheltered) and back (rain-sheltered) stone faces. Atmospheric particles responsible for stone soiling were also analyzed. Results revealed that soot particles (black carbon particles) and soil dust particles were the most abundant particles in the Granada air, intensifying the stone darkening. After the first year of urban exposure, gypsum crusts developed on all stone faces in all tested sites (except in the least polluted one). Calculated total soiling (ΔL^*) corroborated black soiling of stones in all sites, though particularly at the most polluted areas and on rain-unsheltered (front) stone faces. In fact, on front faces surface roughness was higher than in back faces, fostering more intense differential erosion which in turn promotes a feedback process that would trigger further black soiling.

In a two years time span of exposure to the urban environment of Granada, almost all porous limestone surfaces, surpassed the 2% EAC value (percentage of stone area covered by black particles or effective area coverage) considered to be the limit perceptible for the human eye. Indeed the EAC values obtained in this work ranged from 7.8 to 20.4%. It was found that the soiling coefficient calculated based on BC concentration and assuming a square-root fitting shows a relatively constant value for unsheltered surfaces ($8.0–9.9\times10^{-3}$ days$^{-1/2}$ μg$^{-1/2}$ m$^{3/2}$). On the contrary, SC values based on PM10 are more scattered (2.8 to 6.0×10^{-2} days$^{-1/2}$ μg$^{-1/2}$ m$^{3/2}$) suggesting that BC concentration describe more precisely the soiling processes. The soiling evolution of rain-sheltered surfaces is more difficult to evaluate indicating that the balance between deposition and removal of blackening particles and other non-constrained processes strongly differs from site to site for such kind of stone surfaces. This type of study should help restorers to be aware of the most vulnerable areas for architectural stones in polluted cities. Also these data can be potentially used as a first approximation for planning efficient cleaning policies, although longer period of time are required to provide quantitative data to estimate frequency of cleaning actions.

Acknowledgments

Financial support for this work was provided by the Andalusian Research Group RNM-179. M. Urosevic acknowledges the Spanish Ministry of Innovation, Science and Technology for additional financial support through a FPU grant (AP2006-036). The authors thank to H. Lyamani and L. Alados-Arboledas from the Andalusian Center for Environmental Studies (CEAMA) for supplying the annual reports of the air quality in Granada. The authors are thankful also to A. Kowalski for English revision, M.M. Abad from the Scientific Instrumentation Center (CIC) of the University of Granada for HREM analyses of atmospheric particles, two anonymous referees for their constructive reviews and insightful comments and J. Farmer for editorial management.

References

Beloin NJ, Haynie FH. Soiling of building surfaces. J Air Pollut Control Assoc 1975;25: 393–403.

Böke H, Göktürk EH, Caner-Saltik EN, Demirci S. Effect of airborne particle on SO_2-calcite reaction. Appl Surf Sci 1999;140:70–82.

Böke H, Hale Göktürk EH, Caner Saltik EN. Effect of some surfactants on SO_2-marble reaction. Mater Lett 2002;57:935–9.

Bonazza A, Sabbioni C, Ghedini N. Quantitative data on carbon fractions in interpretation of black crusts and soiling on European built heritage. Atmos Environ 2005;39:2607–18.

Bonazza A, Brimblecombe P, Grossi CM, Sabbioni C. Carbon in black crusts from the Tower of London. Environ Sci Technol 2007;41:4199–204.

Bonazza A, Messina P, Sabbioni C, Grossi CM, Brimblecombe P. Mapping the impact of climate change on surface recession of carbonate buildings in Europe. Sci Total Environ 2009;407:2039–50.

Brimblecombe P. Environment and architectural stone. In: Siegesmund S, Snethlage R, editors. Stone in Architecture: Properties, Durability. Springer; 2011. p. 317–46.

Brimblecombe P, Grossi CM. The rate of darkening of material surfaces. In: Saiz-Jimenez C, editor. Air Pollution and Cultural Heritage. Rotterdam: A.A. Balkema; 2004. p. 193–8.

Brimblecombe P, Grossi CM. Aesthetic thresholds and blackening of stone buildings. Sci Total Environ 2005;349:175–89.

Brimblecombe P, Grossi CM. Damage to buildings from future climate and pollution. NAPT Bull 2007;38:13–8.

Brimblecombe P, Grossi CM. Millennium-long damage to building materials in London. Sci Total Environ 2009;407:1354–61.

Camuffo D, Del Monte M, Ongaro A. The pH of the atmospheric precipitation in Venice, related to both the dynamics of precipitation events and the weathering of monuments. Sci Total Environ 1984;40:125–39.

Cardell C. Cristalización de sales en calcarenitas: aplicación al monasterio de San Jerónimo, Granada (Spain). PhD Thesis. Granada: Dept. Mineralogy and Petrology, University of Granada, 1998.

Cardell C, Vleugels G, Torfs K, Van Grieken R. The processes dominating Ca dissolution of limestone when exposed to ambient atmospheric conditions as determined by comparing dissolution models. Environ Geol 2002;43:160–71.

Cardell C, Benavente D, Rodriguez-Gordillo J. Weathering of limestone building material by mixed sulfate solutions. Characterization of stone microstructure, reaction products and decay forms. Mater Charact 2008;59:1371–85.

Cardell C, Guerra I, Romero-Pastor J, Cultrone G, Rodriguez-Navarro A. Innovative analytical methodology combining micro-X-ray diffraction, scanning electron microscopy-based mineral maps, and diffuse reflectance infrared Fourier transform spectroscopy to characterize archeological artifacts. Anal Chem 2009a;81:604–11.

Cardell C, Guerra I, Sánchez-Navas A. SEM-EDX at the service of archaeology to unravel historic technology. Microsc Today 2009b;17:28–33.

Charola AE, Ware R. Acid deposition and the deterioration of stone: a brief review of a broad topic. Geol Soc Lond Spec Publ 2002;205:393–406.

Creighton PJ, Lioy PJ, Haynie FH, Lemmons TJ, Miller JL, Gerhart J. Soiling by atmospheric aerosols in an urban industrial area. J Air Waste Manag Assoc 1990;40:1285–9.

Delalieux F, Cardell-Fernández C, Torfs K, Vleugels G, Van Grieken R. Damage functions and mechanism equations derived from limestone weathering in field exposure. Water Air Soil Pollut 2002;139:75–94.

Doehne E. Salt weathering: a selective review. In: Siegesmund S, Weiss T, Vollbrecht A, editors. Natural Stone, Weathering Phenomena, Conservation Strategies and Cases StudiesGeological Society of London, Special Publications; 2002. p. 51–64.

Doehne E, Price C. Stone conservation: an overview of current research. 2nd ed. Los Angeles: Getty Conservation Institute; 2010.

Esbert RM, Daz-Pache F, Grossi CM, Alonso FJ, Ordaz J. Airborne particulate matter around the Cathedral of Burgos (Castilla y Leon, Spain). Atmos Environ 2001;35:441–52.

Filippou M, Fasseas C, Karabourniotis G. Photosynthetic characteristics of olive tree (*Olea europaea*) bark. Tree Physiol 2007;27:977–84.

Folk RL. The petrology of sedimentary rocks. Austin, Texas: Hemphill Publishing Company; 1981.

Ghedini N, Sabbioni C, Bonazza A, Gobbi G. Chemical–thermal quantitative methodology for carbon speciation in damage layers on building surfaces. Environ Sci Technol 2006;40:939–44.

Grossi CM, Brimblecombe P. Aesthetics of simulated soiling patterns on architecture. Environ Sci Technol 2004;38:3971–6.

Grossi CM, Brimblecombe P. Effect of long-term changes in air pollution and climate on the decay and blackening of European stone buildings. Geol Soc Lond Spec Publ 2007;271:117–30.

Grossi CM, Brimblecombe P. Past and future colouring patterns of historic stone buildings. Rev Mater Construct 2008;58:143–60.

Grossi CM, Esbert RM, Díaz-Pache F, Alonso FJ. Soiling of building stones in urban environments. Build Environ 2003;38:147–59.

Grossi CM, Brimblecombe P, Esbert RM, Alonso FJ. Color changes in architectural limestones from pollution and cleaning. Color Res Appl 2007;32:320–31.

Hamilton R, Crabbe H. Environment, pollution and effects. In: Watt J, Tidblad J, Kucera V, Hamilton R, editors. The Effects of Air Pollution on Cultural Heritage. Boston, MA: Springer; 2009. p. 1-28.

Hamilton RS, Mansfield TA. The soiling of materials in the ambient atmosphere. Atmos Environ A 1992;26:3291–6.

Horemans B, Cardell C, Laszlo Bencs, Kontozova-Deutsch V, De Wael K, Van Grieken R. Evaluation of airborne particles at the Alhambra monument in Granada, Spain. Microchem J 2011;99:429–38.

Katrinak KA, Anderson JR, Buseck PR. Individual particle types in the aerosol of Phoenix, Arizona. Environ Sci Technol 1995;29:321–9.

Kindratenko VV, Van Espen PJM, Treiger BA, Van Grieken R. Fractal dimensional classification of aerosol particles by computer-controlled scanning electron microscopy. Environ Sci Technol 1994;28:2197–202.

Kontozova-Deutsch V, Cardell C, Urosevic M, Ruiz-Agudo E, Deutsch F, Van Grieken R. Characterization of indoor and outdoor atmospheric pollutants impacting architectural monuments: the case of San Jerónimo Monastery (Granada, Spain). Environ Earth Sci 2011;63:1433–45.

Kucera V. Model for multipollutant impact and assessment of threshold levels for cultural heritage. Stockholm: Swedish corrosion Institute; 2005.

Lyamani H, Bravo Aranda JA. Informe de calidad del aire de Granada: año 2008. Informe interno. Granada (Spain): Universidad de Granada; 2009.

Lyamani H, Bravo Aranda JA. Informe de calidad del aire de Granada: año 2009. Informe interno. Granada (Spain): Universidad de Granada; 2010.

Lyamani H, Olmo FJ, Alados-Arboledas L. Long-term changes in aerosol radiative properties at Armilla (Spain). Atmos Environ 2004;38:5935–43.

Lyamani H, Olmo FJ, Alados-Arboledas L. Light scattering and absorption properties of aerosol particles in the urban environment of Granada, Spain. Atmos Environ 2008;42:2630–42.

Lyamani H, Olmo FJ, Alados-Arboledas L. Physical and optical properties of aerosols over an urban location in Spain: seasonal and diurnal variability. Atmos Chem Physics 2010;10:239–54.

Maravelaki-Kalaitzaki P. Black crusts and patinas on Pentelic marble from the Parthenon and Erechtheum (Acropolis, Athens): characterization and origin. Anal Chim Acta 2005;532:187–98.

Maravelaki-Kalaitzaki P, Biscontin G. Origin, characteristics and morphology of weathering crusts on Istria stone in Venice. Atmos Environ 1999;33:1699–709.

Merinero R, Lunar R, Somoza L, Diaz-del-Rio V, Martinez-Frias J. Nucleation, growth and oxidation of framboidal pyrite associated with hydrocarbon-derived submarine chimneys: lessons learned from the Gulf of Cadiz. Eur J Mineral 2009;1:947–61.

Murr LE, Bang JJ. Electron microscope comparisons of fine and ultra-fine carbonaceous and non-carbonaceous, airborne particulates. Atmos Environ 2003;7:4795–806.

Pio CA, Ramos MM, Duarte AC. Atmospheric aerosol and soiling of external surfaces in an urban environment. Atmos Environ 1998;2:1979–89.

Pósfai M, Buseck PR. Nature and climate effects of individual tropospheric aerosol particles. Annu Rev Earth Planet Sci 2010;8:17–43.

Pósfai M, Anderson JR, Buseck PR, Sievering H. Soot and sulfate aerosol particles in the remote marine troposphere. J Geophys Res Lett 1999;104:21685–93.

Querol X, Alastuey A, Viana MM, Rodriguez S, Artiñano B, Salvador P, et al. Speciation and origin of PM10 and PM2.5 in Spain. J Aerosol Sci 2004;5:1151–72.

Rodríguez-Navarro C. Causas y mecanismos de alteración de los materiales calcáreos de las catedrales de Granada y Jaén. Tesis Doctoral. Granada: Universidad de Granada, 1994. 435 pp.

Rodríguez-Navarro C, Sebastián E. Role of particulate matter from vehicle exhaust on porous building stones (limestone) sulfation. Sci Total Environ 1996;87:79–91.

Rodríguez-Navarro C, Sebastián-Pardo E, Ruiz-Agudo E. Plan Director del Hospital Real: Estudio de materiales, formas y mecanismos de alteración. Informe interno. Granada: Universidad de Granada; 2008.

Sabbioni C. Mechanisms of air pollution damage to stone. In: Brimblecombe P, editor. Effects of Air Pollution on the Built Environment. Singapore: Imperial College Press; 2003. p. 63-106.

Sabbioni C, Zappia G. Atmospheric-derived element tracers on damaged stone. Sci Total Environ 1992;126:35–48.

Sabbioni C, Ghedini N, Bonazza A. Organic anions in damage layers on monuments and buildings. Atmos Environ 2003;37:1261–9.

Scherer GW. Crystallization in pores. Cem Concr Res 1999;29:1347–58.

Siegesmund S, Snethlage R. Stone in architecture: properties, durability. 4th Edition. Springer; 2011.

Simão J, Ruiz-Agudo E, Rodriguez-Navarro C. Effects of particulate matter from gasoline and diesel vehicle exhaust emissions on silicate stones sulfation. Atmos Environ 2006;40:6905–17.

Urosevic M, Sebastián-Pardo E, Ruiz-Agudo E, Cardell C. Physical properties of carbonate rocks used as a modern and historic construction material in Eastern Andalusia, Spain. Mat Constr 2011;61:93-114.

Vendrell-Saz M, Garcia-Vallès M, Alarcón S, Molera J. Environmental impact on the Roman monuments of Tarragona, Spain. Environ Geol 1996;27:263–9.

Viles HA. Can stone decay be chaotic? Geol Soc Am Spec Pap 2005;390:11–6.

Viles HA, Gorbushina AA. Soiling and microbial colonisation on urban roadside limestone: a three year study in Oxford, England. Build Environ 2003;38:1217–24.

Viles HA, Taylor MP, Yates TJS, Massey SW. Soiling and decay of N.M.E.P. limestone tablets. Sci Total Environ 2002;292:215–29.

Völz HG. Industrial color testing: fundamentals and techniques. 2nd Edition. Wiley-VCH; 2001.

Watt J, Tidblad J, Kucera V, Hamilton R. The effects of air pollution on Cultural Heritage. Springer; 2009.

Wyszecki G, Stiles WS. Colour science. Concepts and methods, quantitative data and formulae2nd ed. New York: J. Wiley & Sons; 1982.

Xie Y, Hopke PK, Wienke D. Airborne particle classification with a combination of chemical composition and shape index utilizing an adaptive resonance artificial neutral network. Environ Sci Technol 1994;28:1921–8.